International Conference on Artificial Reality and Telexistence
Eurographics Symposium on Virtual Environments (2023)
J.-M. Normand, M. Sugimoto, and V. Sundstedt (Editors)

Analyzing the Behavior of Projector-Camera Systems Based on Reaction-Diffusion Equations

Toshiyuki Amano[†1]

[1]Graduate School of Systems Engineering, Wakayama University, Japan

Abstract

Pixel Feedback Animation (PFA), a technique that uses projector-camera feedback, has emerged as a dynamic illumination method introducing variations in color and brightness for expressive purposes. Notably, the deliberate application of specific image processing techniques during the projector-camera feedback loop has unveiled the potential to generate patterns reminiscent of Turing patterns solutions to reaction-diffusion equations. However, the intrinsic nature of PFA's projection-camera system consists of image capture and reflective properties of the projection surface, which create illumination patterns. In this paper, a comprehensive investigation into the underlying mechanisms of PFA is presented, revealing its inherent connection to reaction-diffusion systems. The study explores the emergence of distinct PFA patterns intricately influenced by variations in object surface reflectivity and coloration.

CCS Concepts

• ***Human-centered computing*** → ***Mixed / augmented reality;*** • ***Computing methodologies*** → ***Mixed / augmented reality;***

1. Introduction

The concept of Spatial Augmented Reality (SAR), enabling real-world Augmented Reality (AR) through projector-based projection, was introduced by Raskar with Shader Lamps [RWLB01]. Since then, SAR research has focused on three essential requirements for AR: geometric consistency, optical consistency, and temporal consistency. These requirements encompass various aspects such as compensating for projection blur, tracking moving or deforming objects, and ensuring alignment with the real world [GI18]. As an application, SAR holds unique potential, allowing users to experience AR directly in the real world without the need for head-mounted displays or intermediary mobile devices. This capability also promises to introduce a mirrored world into the real world while preserving its authenticity.

In the context of SAR, radiometric compensation techniques have been explored. These include optical compensation to accurately display desired images with correct coloration on patterned wall surfaces [GPNB04] and methods considering human perception [AOSS06]. In contrast, a technique for appearance manipulation, aiming to enhance or transform the appearance of objects, has also been explored. Research in this area has focused on tasks such as optically restoring deteriorated artworks [ALY08], presenting high dynamic range images [SIS11], and manipulating the expressiveness of mannequins [BBG*13]. Additionally, Deformation Lamps [KFSN16], which apply perceptual deformation with vision theory, have been proposed.

One specific method within SAR is the concept of 'Appearance Control,' which we proposed and employed optical feedback systems with projectors and cameras [AK10b]. This technique has found applications in visual assistance [AK10a], material appearance manipulation [Ama13, Ama19], optical illusions [Ama12, Ama16], and more. Moreover, it extends its applications beyond research boundaries, offering opportunities in installation art. For installation art applications, a novel technique called Pixel Feedback Animation (PFA) has been proposed [ASH18]. PFA introduces fluctuations in color and brightness as expressive elements. The behavior of PFA varies depending on the image processing algorithms and parameters used in target image generation. Notably, applying specific image processing for target image generation can lead to patterns similar to Turing patterns, which are solutions to reaction-diffusion equations. However, the inherent image capture in its projection-camera system intricately intertwines with the reflection characteristics of the projection target, influencing the resulting patterns.

This paper uncovers the connection between PFA and reaction-diffusion systems and explores pattern generation driven by variations in object surface reflectivity and coloration using PFA.

† amano@wakayama-u.ac.jp

DOI: 10.2312/egve.20231308

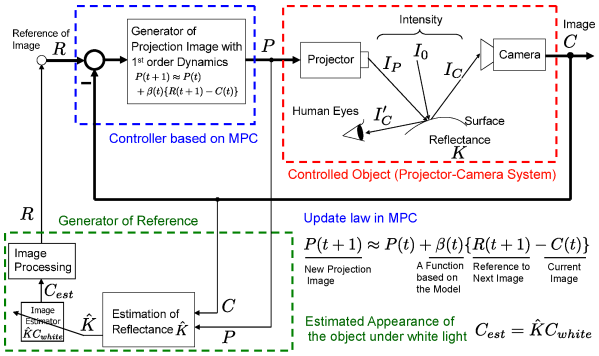

Figure 1: *Diagram showing the appearance control technique. The process is divided into three main parts: a controlled object, a controller that employs model predictive control, and a reference generator. The most important component is the reference generator, which allows adaptive scene appearance manipulation in a similar manner to photo retouching software.*

2. Appearance Control

Appearance control, as illustrated in the diagram in Figure 1, is an optical feedback system that achieves manipulation of appearance through camera capture and projector projection. At a specific point on an object's surface, the reflected light $\mathbf{I}_C$ is described as

$$\mathbf{I}_C = \mathrm{K}(\mathbf{I}_P + \mathbf{I}_0), \tag{1}$$

where $\mathbf{I}_0$ and $\mathbf{I}_P$ are environmental illumination and projection from the projector. These are represented as RGB color vectors and described within a 3×3 matrix denoting reflectance as K.

Assuming linearity in the optical responses of both the camera and projector on the corresponding image coordinate (x_c, y_c) and (x_p, y_p), reflectance can be accurately estimated by

$$\hat{\mathrm{K}} = \mathrm{diag}\left\{\mathbf{C}./(\mathbf{MP} + \mathbf{C}_0)\right\}. \tag{2}$$

where $./$ denotes element-wise division, $\mathrm{M} \in \mathbb{R}^{3\times3}$ represents a color mixing matrix essential for harmonizing color alignment between the projector and camera. This estimation relies pixel on captured image $\mathbf{C}(x_c, y_c) \in \mathbb{R}^3$, projected image $\mathbf{P}(x_p, y_p) \in \mathbb{R}^3$, and an image acquired under conditions without projection $\mathbf{C}_0(x, y)$. Its calibration is performed in advance using a whiteboard.

Subsequently, the apparent appearance under white illumination $\mathbf{C}_{\mathrm{est}}$ is generated by modulating a white image with $\hat{\mathrm{K}}$. Then, the desired image processing is then applied to $\mathbf{C}_{\mathrm{est}}$ to attain the control reference $\mathbf{R}$. In the feedback loop, $\mathbf{P}$ is adjusted to the difference between $\mathbf{R}$ and $\mathbf{C}$ is reduced through a model predictive controller. This adjustment allows for the manipulation of $\mathbf{I}_C$ into the desired visual appearance dictated by the provided image processing. Notably, under the assumption of diffuse reflection on the surface, the color $\mathbf{I}'_C$ perceived by the observer perspective closely matches $\mathbf{I}_C$.

3. Pixel Feedback Animation (PFA)

In December 2015, during the solo exhibition "Memories of the Moon" by Hiroto Rakusho, held at the Mitsukoshi Department Store in Japan, a novel technique PFA was developed for the projection mapping onto the brocade tapestry titled "Moonlight" as shown in Figure 2. This technique has introduced dynamic variations into the projection patterns.

PFA is a unique artistic technique that achieves dynamic visual effects by deliberately setting image processing parameters to induce instability within the control system. It relies on the interplay between image processing and the optical feedback loop involving camera capture and projector projection. The reflective properties of the target surface serve as boundary conditions for generating intricate patterns based on the chosen image processing settings.

For instance, the (a) reflection effect, which reveals glossiness, is created by applying brightness normalization on the estimated original appearance while deliberately amplifying the contrast through parameter settings. This results in the emergence of cloud-like textures influenced by the tapestry's patterns, with alternating brightness over time. The (b) Bubble Effect is achieved by implementing excessive edge enhancement followed by contrast enhancement in the image processing. This parameter configuration leads to the propagation of light ripple patterns reminiscent of growing bubbles due to fine surface structures on the tapestry. The (c) Blue Earth Effect, named for its resemblance to Earth's appearance from space, combines hue manipulation with exceeding contrast enhancement. This results in a shifting overall color tone and saturation changes. These areas correspond to the reflective properties of the tapestry. The (d) Rainbow Effect creates a dynamic color transformation over time by excessive parameters for monochromatic conversion. In (e) No Title #2, intense color oscillations are induced by converting high-saturation regions to desaturated colors and vice versa. Lastly, (f) No Title #3, unlike the Bubble Effect, maintains proper parameter settings for edge enhancement but exceeds contrast manipulation, leading to a gentle spread of light blurring patterns caused by the tapestry's patterns.

Compared to nonlinear video feedback [HSW85], PFA exhibits spatial-temporal dynamics by common factors such as processing delay and optical blurring. A distinguished characteristic of PFA is its projection onto the target surface, which results in imagery modulation by the surface texture. This study explores the creative possibilities of PFA with an example of projection onto brocade tapestries, showcasing its potential for generating captivating and dynamic visual effects.

4. Reaction and Diffusion Terms in Projection Camera Feedback System

4.1. Reaction-Diffusion Equations

The two-variables reaction-diffusion equation describes the behavior on the spatial coordinate (u, v) at time t by the coupled partial differential equations with reaction terms $F(u, v), G(u, v)$ and diffusion terms $\nabla^2 u, \nabla^2 v$ by

$$\begin{cases} \frac{\partial u}{\partial t} = F(u,v) - du + D_u \nabla^2 u \\ \frac{\partial v}{\partial t} = G(u,v) - gv + D_v \nabla^2 v \end{cases} \tag{3}$$

where D_u and D_v represent the diffusion coefficients, and ∇^2 is the Laplacian operator. Alan Turing demonstrated that in such a two-

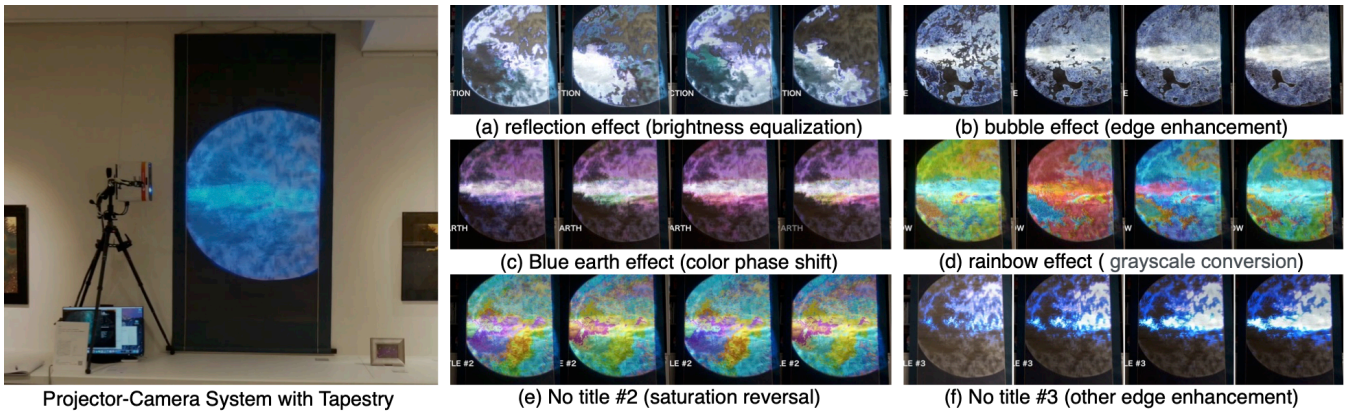

Figure 2: *Dynamic Visual Effects with Pixel Feedback Animation (PFA). PFA introduces dynamic variations into projection patterns by deliberately inducing instability within the control system, relying on the interplay between image processing and an optical feedback loop involving camera capture and projector projection.*

variable system, spatial patterns, known as Turing patterns, spontaneously emerge when D_u and D_v are significantly different, and $F(u,v)$ and $G(u,v)$ meet certain conditions [Tur52]. Even when not relying on such partial differential equations, implementing algorithms analogous to activators and inhibitors can produce Turing patterns using cellular automata [SM92].

As explained in Section 3 regarding the PFA's Bubble Effect, the projection-camera system induces patterns similar to Turing patterns using the object's patterns as boundary conditions, as illustrated in Figure 3. In optical feedback systems employing projectors and cameras, both the object under manipulation and internal system characteristics or processes act as the diffusion and reaction terms, contributing to the emergence of Turing patterns.

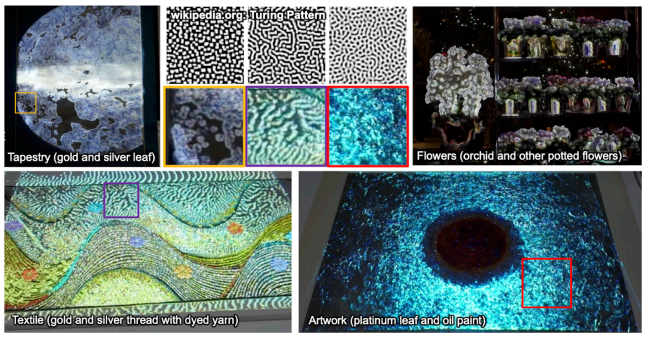

Figure 3: *Turing Pattern-Like Effects. This figure illustrates the emergence of Turing pattern-like effects in projection-camera systems. These effects arise from the interaction between the manipulated object and the system's internal characteristics.*

4.2. Diffusion and Reaction Terms in Image Processing

In the Bubble Effect, PFA employed an edge enhancement in the image processing. For each pixel on (x,y), following operation to each channel of the estimated image $\mathbf{C}_{\text{est}} = \{C^r_{\text{est}}, C^g_{\text{est}}, C^b_{\text{est}}\}$ under white illumination generates target image,

$$\mathbf{R}(x,y) = f(\text{gain}\{\text{sat}\nabla^2\mathbf{C}_{\text{est}}(x,y) + (1-\text{sat})\mathbf{C}_{\text{est}}(x,y)\}) \quad (4)$$

where, gain and sat are image processing parameters, and $f(\cdot)$ represents contrast enhancement. Typically, values are significantly larger in image differentiation at edge regions while close to zero elsewhere. Therefore, the edge image component is less affected by the non-linear transformation introduced by $f(\cdot)$. Additionally, $\mathbf{C}_{\text{est}}$ is calculated as the product of the color $\mathbf{C}_w$ under white reference board and $\hat{\mathbf{K}}$. Based on these considerations, Equation (4) can be approximated using appropriate coefficients a and b as

$$\mathbf{R}(x,y) \approx a\nabla^2\hat{\mathbf{K}}(x,y)\mathbf{C}_w + bf(\hat{\mathbf{K}}(x,y)\mathbf{C}_w). \quad (5)$$

Thus, in the target image generation of the Bubble Effect, there is a structure with $\nabla^2\hat{\mathbf{K}}(x,y)\mathbf{C}_w$ as the diffusion term and $bf(\hat{\mathbf{K}}(x,y)\mathbf{C}_w)$ as the reaction term. When there is no motion in the scene, the estimated reflectance $\hat{\mathbf{K}}(x,y)$ should ideally remain invariant over time. However, practical projector-camera systems introduce a delay in $\mathbf{C}$, which results in temporal variations in $\hat{\mathbf{K}}(x,y)$. This temporal variation in $\hat{\mathbf{K}}(x,y)$ is considered one factor contributing to the dynamics of the reaction-diffusion system.

As explained in Section 3, all PFA methods exhibit dynamics such as projection flickering due to excessive parameter settings. However, among the examples shown in Figure 2, only the Bubble Effect produces Turing patterns. While the formation of Turing patterns requires both diffusion and reaction terms to be present, target image generation methods other than the Bubble Effect lack the diffusion term seen in Eq.(5). Therefore, $\hat{\mathbf{K}}(x,y)$ varies over time, and $\mathbf{R}(x,y)$ includes diffusion terms as shown in Eq.(5) is required to generate produces Turing pattern like effects.

4.3. Diffusion Components in Object Surface

In actual reflections from the object of interest, it is essential to consider not only the direct reflection K from the object's surface but

also multiple reflections and subsurface scattering caused by complex structures. Moreover, optical blurring occurs due to the projection from the projector and the capturing by the camera. Additionally, geometric transformations (Geometry Transform) for accurate pixel correspondence between the projected and captured scenes introduce variations at sub-pixel levels.

The correspondence relationship between the projected image $\mathbf{P}$ and the captured image $\mathbf{C}$, considering such scattering and variations, can be described using the light transport matrix [PBG*05]. If we arrange the pixels of the projected image $\mathbf{P}(x_p, y_p)$ and the captured image $\mathbf{C}(x_c, y_c)$, both placed on a two-dimensional grid into vectors $\mathbf{p}$ and $\mathbf{c}$, respectively. In the scenario where $\mathbf{I}_0 = 0$, the relationship between the projected and captured images can be represented using a light transport matrix T as

$$\mathbf{c} = \mathrm{T}\mathbf{p} \tag{6}$$

where, the dimensions of $\mathbf{p}$ and $\mathbf{c}$ correspond to the number of pixels in each image.

When the direct reflection component of light projected from a pixel (x_p, y_p) in $\mathbf{P}$ is observed at a pixel (x_c, y_c) in $\mathbf{C}$, this correspondence relationship can be described using D_G. Moreover, we can represent the spreading of light due to subsurface scattering as an excess component D_Δ, and the light transport matrix can be rewritten as

$$\mathrm{T} = \mathrm{K}(\mathrm{D}_G + \mathrm{D}_\Delta). \tag{7}$$

Here, D_G is a permutation matrix that places a 1 in (x_c, y_c) corresponding to (x_p, y_p), and 0 otherwise in each row, defined as following delta function

$$\delta(x_c, y_c; x, y) = \delta(x - x_p(x_c, y_c))\delta(y - y_p(x_c, y_c)), \tag{8}$$

where $x_p(x_c, y_c)$, $y_p(x_c, y_c)$ are pixel mapping. Additionally, uniform subsurface scattering, which causes light to spread around (x_c, y_c), can be represented through convolution with an appropriate kernel

$$d_\Delta(x_c, y_c). \tag{9}$$

Therefore, as an image operation is

$$\mathbf{C}(x_c, y_c) = \mathrm{K}(x_c, y_c)\left(\mathbf{P}'(x_c, y_c) + d_\Delta * \mathbf{P}'(x_c, y_c)\right), \tag{10}$$

where $\mathbf{P}'$ is the image transformed from $\mathbf{P}$ using $\delta(x_c, y_c; x, y)$

$$\begin{aligned}\mathbf{P}'(x_c, y_c) &= \sum_{y_p}\sum_{x_p}\delta(x_c, y_c; x_p, y_p)\mathbf{P}(x_p, y_p) \\ &= \mathbf{P}(x_p(x_c, y_c), y_p(x_c, y_c)),\end{aligned} \tag{11}$$

and * represents convolution.

When the blurring of reflected light caused by direct reflection and subsurface scattering follows an isotropic Gaussian function, we can determine $\mathrm{K}(x_c, y_c)$ so that

$$\sum_u \sum_v d'_\Delta(u, v) = 0, \tag{12}$$

where d'_Δ becomes the difference between Gaussian functions with different variances, approximating ∇^2. Thus, for a reflective surface that includes subsurface scattering, we can consider the composition of the diffusion term and the proportional term in the reaction-diffusion system as

$$\mathbf{C}(x_c, y_c) = \mathrm{K}(x_c, y_c)\left(\mathbf{P}'(x_c, y_c) + \nabla^2\mathbf{P}'(x_c, y_c)\right). \tag{13}$$

Here, $C(x_c, y_c)$, $P(x_p, y_p)$, and $P'(x_c, y_c)$ represent color images with RGB values, and the operations above are performed separately for each RGB channel.

4.4. Reaction Components in Color Alignment

In general, the color spaces of projectors and cameras do not match. For example, projecting a pure red image from the projector results in responses observed in all RGB channels in the captured image. Therefore, for estimating the reflectance, the observed projection image's color is modeled using the color mixing matrix M as

$$\hat{\mathbf{C}}(x_c, y_c) = \mathrm{M}\mathbf{P}'(x_c, y_c) + \mathbf{C}_0(x_c, y_c) \tag{14}$$

where $\mathbf{C}_0(x_c, y_c)$ represents the environmental illumination component. In other words, with M as weights, this transformation mixes RGB components, generating a reaction term that introduces interactions in a three-variable system with each RGB component as a variable.

5. Description of PFA as a Reaction-Diffusion Equation

5.1. Model Predictive Control (MPC)

The appearance control employed a Model Predictive Controller (MPC) that conducts one-step prediction [GPM89] using estimated reflectance and color mixing matrix-based response models for each pixel. The projection image is updated to minimize the difference from the reference trajectory. The update of the projection image using MPC can be expressed as

$$\mathbf{P}(t+1) \approx \mathbf{P}(t) + \beta(t)\left(\mathbf{R}(t+1) - \mathbf{C}(t)\right). \tag{15}$$

Here, assuming the time unit to be sufficiently small, it can be rewrite as

$$\frac{\partial \mathbf{P}}{\partial t}(t) \approx \beta(t)\left(\mathbf{R}(t+1) - \mathbf{C}(t)\right). \tag{16}$$

5.2. PFA's Reaction and Diffusion Components

From Eq.(16) and Eq.(10), we can describe PFA dynamics as

$$\begin{aligned}\frac{\partial \mathbf{P}}{\partial t}(t; x, y) &\approx \beta(t; x, y) \\ &\times \left(\mathbf{R}(t+1; x, y) - \mathrm{K}(t; x, y)\left(\mathbf{P}(t; x, y) + \nabla^2\mathbf{P}(t; x, y)\right)\right).\end{aligned} \tag{17}$$

Here, assuming a stationary scene, $\mathrm{K}(t; x, y) = \mathrm{K}(x, y)$ and $\mathbf{R}(t+1; x, y) = \mathbf{R}(x, y)$. Also, in the case of a sufficiently long time, the system reaches a steady state, and $\beta(t; x, y) \to \beta(x, y)$,

$$\begin{aligned}\frac{\partial \mathbf{P}}{\partial t}(t; x, y) \approx{}& \beta(x, y)\mathbf{R}(x, y) - \beta(x, y)\mathrm{K}(x, y)\mathbf{P}(t; x, y) \\ &- \beta(x, y)\mathrm{K}(x, y)\nabla^2\mathbf{P}(t; x, y).\end{aligned} \tag{18}$$

From the above, PFA can be described as a reaction-diffusion system with the reaction term:

$$-\beta(x, y)\mathrm{K}(x, y)\mathbf{P}(t; x, y) \tag{19}$$

and the diffusion term:

$$-\beta(x,y)\mathrm{K}(x,y)\nabla^2\mathbf{P}(t;x,y). \tag{20}$$

However, as explained in Section 3, unless excessive parameters are set, perceptual control operates stably without causing flickering in projections. Therefore, only Eq.(19) does not make the system unstable. Moreover, to exhibit Turing patterns, diffusion terms included in the Bubble effect are required, which implies that the reaction term Eq.(19) and the diffusion term Eq.(20) alone do not satisfy the conditions for the emergence of Turing patterns.

Taking into account the delay Δt in capturing images, the estimation of reflectance can be written as a function of time t

$$\hat{\mathrm{K}}(t;x,y) = \mathrm{diag}\Big\{\mathrm{K}(x,y)\Big(\mathbf{P}(t-\Delta t;x,y)+\nabla^2\mathbf{P}(t-\Delta t;x,y)\Big) \Big/ \Big(\mathrm{M}\mathbf{P}(t;x,y)+\mathbf{C}_0\Big)\Big\}, \tag{21}$$

where $\mathbf{P}(t;x,y)$ introduces dynamics into $\hat{\mathrm{K}}(t;x,y)$. Therefore $\hat{\mathrm{K}}(t;x,y)$ can be written as a function which has $\mathbf{P}(t;x,y)$. Additionally, the constant term $\mathbf{R}(x,y)$ in Eq.(18) contains $\hat{\mathrm{K}}$ as shown in Eq.(5). In summary, the reaction term of PFA is:

$$b\,f(\hat{\mathrm{K}}(t;x,y)\mathbf{C}_w) - \beta(x,y)\mathrm{K}(x,y)\mathbf{P}(t;x,y) \tag{22}$$

and the diffusion term is:

$$a\nabla^2\hat{\mathrm{K}}(t;x,y)\mathbf{C}_w - \beta(x,y)\mathrm{K}(x,y)\nabla^2\mathbf{P}(t;x,y). \tag{23}$$

From the above, the mechanism of PFA with edge enhancement processings can be explained as a reaction-diffusion equation.

5.3. Conditions for Turing Pattern Formation with PFA

As evident from Eq.(19) and Eq.(20), the appearance control on the surfaces includes subsurface scattering contains both a reaction term and a diffusion term. However, Turing patterns will not emerge unless the reaction and diffusion terms arising from reflective properties meet specific conditions. To intentionally induce Turing patterns with PFA based on reflective properties, manipulating behavior using image processing that includes both diffusion and reaction terms similar to the Bubble effect is necessary. The edge enhancement process in the Bubble effect involves a second-order differentiation through mask operations, allowing the control of reaction and diffusion terms as shown in Eq.(22) and Eq.(23) based on target image generation parameters.

Turing patterns emerge when diffusion coefficients vary with each variable, and there are differences in diffusion rates. Since PFA is a 3-variable system with each channel of RGB as a variables, promoting the emergence of Turing patterns can be contemplated by interaction among color channels. One opportunity is the adopted image processing, which makes mixing and illumination gain differences in each color channel even if the object color is white. Additionally, color matching between the projector and camera is included in Eq.(21), which results in differences in diffusion for each channel with $\hat{\mathrm{K}}(t;x,y)$ in Eq.(23). Therefore, it is likely that Turing patterns will emerge even when the target image $\mathbf{R}(x,y)$ or the captured image $\mathbf{C}(x,y)$ are monochromatic.

6. Investigation through Simulation

6.1. Reproduction of PFA Using Optical Transport Matrices

PFA has been described as a reaction-diffusion system, and the mechanism of Turing pattern formation is revealed. This section validates this by observing behavior changes while altering the reflective properties of the projection target. This validation necessitates high precision and the ability to manipulate reflective properties flexibly. Therefore, a simulation environment is constructed using light transport matrices, replacing the projector-camera system.

In the model of the projector-camera system, an image $\mathbf{E}(x_c,y_c)$ is obtained under the condition of environmental illumination with $\mathbf{I}_p = 0$ and the projected image $\mathbf{P}(x_p,y_p)$. These images are then converted into vectors $\mathbf{p}$ and $\mathbf{e}$, and computed as:

$$\mathbf{c} = \mathrm{T}\mathbf{p} + \mathbf{e}. \tag{24}$$

To generate the captured image $\mathbf{C}(x_c,y_c)$, the light transport is computed, and the resulting image is then sent to the ring buffer to replicate the time response existing in the actual camera.

The light transport matrix T is computed using Push Broom projection as described in [MTK16]. To simulate PFA, the entire projector-camera system is implemented, as depicted in Figure 4. The projector has a resolution of 1280 800 pixels, the camera has a resolution of 1304 800 pixels, and a delay of 3 frames is introduced via the frame buffer. The light transport matrices were implemented by half resolution for reducing its storage and acquisition cost.

6.2. Exploration of PFA Parameters by Varying Reflective Properties

To discover the condition of the emergence of Turing pattern formation based on differences in reflective properties such as subsurface scattering, several image processing techniques, including image differentiation, were implemented in the simulator mentioned above. Parameters were adjusted to induce Turing patterns. Subsequently, subsurface scattering components were removed from the object surface's reflectance properties with the formula described in 4.3, and PFA behavior was investigated. Furthermore, by analyzing the transformed captured images, the relationship between object surface reflectance and Turing pattern formation was examined. For this simulation, a textile woven with gold and dyed threads, as depicted in Figure 5, is employed.

6.3. Turing Pattern Formation through PFA Simulation

Edge enhancement used LoG (Laplacian of Gaussian) Kernel

$$\mathrm{LoG}(\sigma;x,y) = \nabla^2 \exp\left(-\frac{x^2+y^2}{\sigma^2}\right) \tag{25}$$

and the Wolffsohn's edge enhancement [WMR07] were employed to induce Turing patterns through PFA simulation. Saturation (sat), gain (gain) and contrast (cont) parameters are applied to edge enhancement result $\mathbf{C}_{Edge}(x,y)$ and make reference image $\mathbf{R}$(x,y) as

$$\mathbf{R}'(x,y) = \mathrm{gain}\left\{\mathrm{sat}\mathbf{C}_{Edge}(x,y) + (1-\mathrm{sat})\mathbf{C}_{est}(x,y)\right\}, \tag{26}$$

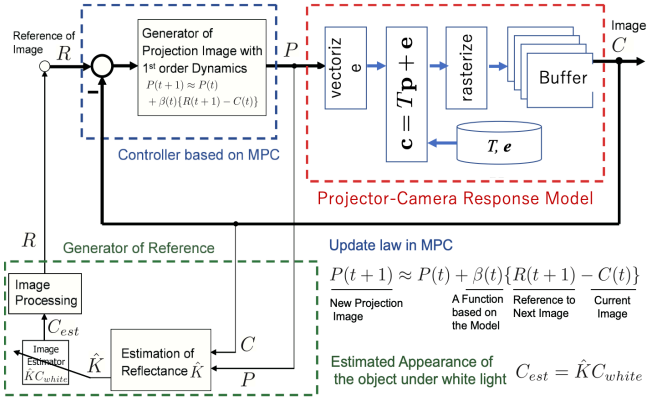

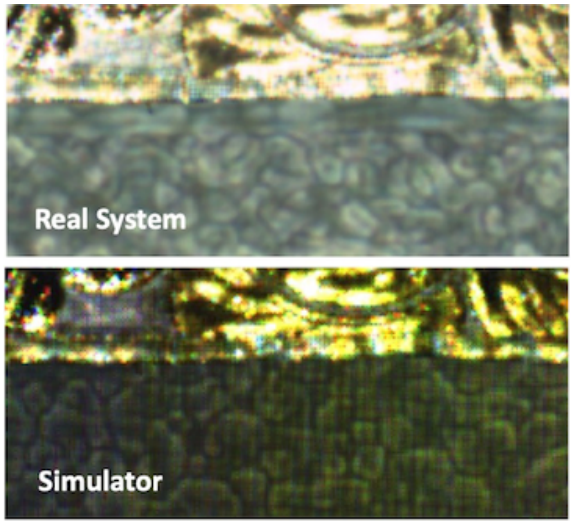

Figure 4: *PFA simulator. The upper figure demonstrates the implementation of a PFA simulator. The optical response between the projector and camera, which includes the geometrical transformation of the projected image, is implemented through the utilization of light transport matrices. A frame delay introduced via a frame buffer ensures the high precision and accurate reproduction of PFA dynamics. Despite the limited resolution of light transport matrices, we can observe a Turing pattern-like effect reproduced successfully with this simulator, as shown in the bottom figure.*

$$\mathbf{R}(x,y) = \mathbf{R}'(x,y)^{\text{cont}}. \tag{27}$$

Figure 6 shows an enlarged view of $\mathbf{C}(x,y)$ under the condition where PFA converges sufficiently (t is sufficiently large). In (b)-(d), Wolffsohn's edge enhancement was applied to monochrome-transformed $\mathbf{C}_{est}(x,y)$, and color was added by multiplying the weight of the color vector $\mathbf{d}$. The parameters used for these patterns are presented in Table 1.

6.3.1. Changes in Behavior by Removing Subsurface Scattering (Condition I)

At first the sum of each row in the light transport matrix T is calculated and determined the reflectance value of K as shown in Eq.

Figure 5: *Gold and Dyed Thread Woven Textile.*

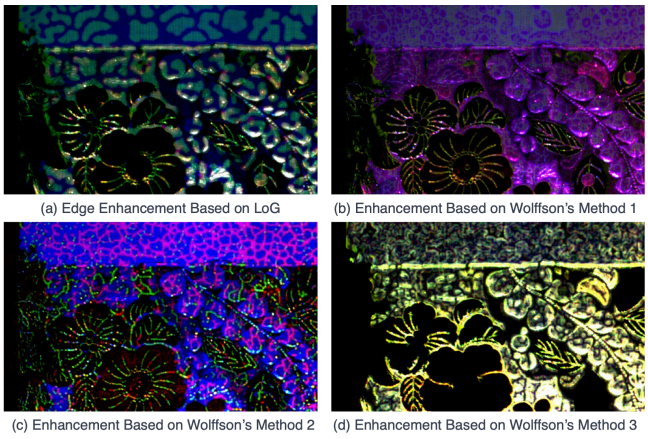

Figure 6: *Turing Pattern Formation in PFA Simulation. This figure illustrates the formation of Turing patterns in a PFA simulation through edge enhancement techniques, including LoG (Laplacian of Gaussian) and Wolffsohn's method.*

(7). Subsequently, the direct reflection D_G is extracted by selecting the column with the maximum value and setting it to 1. Then the subsurface scattering component is decomposed as follows:

$$\mathrm{D}_\Delta = \mathrm{K}^{-1}\mathrm{T} - \mathrm{D}_G. \tag{28}$$

After this decomposition, the matrix T is reconstructed by setting D_Δ to 0, and a PFA simulation is then conducted. This allowed us to investigate how the presence or absence of subsurface scattering affects the system's behavior.

6.3.2. Changes in Behavior by Removing Object Surface Coloration (Condition II)

In this study, the projector-camera system is described as a 3-variable reaction-diffusion system, with each RGB channel serving as an individual variable. For Turing patterns to emerge in the reaction-diffusion system, it is necessary that the diffusion coefficients of each variable must differ significantly. These diffusion coefficients also vary within the light transport matrix T, as demonstrated in Eq. (7) in addition to the image processing. Therefore, this paper examines changes in behavior when the coloration of

Table 1: *PFA parameters*

	(a) LoG based	(b) Wolffsohn1	(c) Wolffsohn2	(d) Wolffsohn3
σ	5.0	2.0	2.0	2.0
gain	0.31	0.45	0.60	0.65
sat	-0.26	1.00	-0.50	1.70
cont	0.02	0.00	0.02	1.00
d (R,G,B)	-	(0,0,1)	(1,1,1)	(1,1,1)

the object surface differs by transforming the captured images into monochrome.

Figure 7 shows the differences in $\mathbf{P}(x,y)$ between the original condition where reflective properties were not manipulated ("Original") and when reflective properties were manipulated using both Condition I and Condition II. For this simulation, four image processing algorithms with specific parameters that induce Turing patterns, as depicted in Figure 6, are applied.

7. Discussion

In Figure 7, Turing patterns are generated even when Condition I is applied, as shown in (a). However, upon applying Condition II, ripples in areas devoid of patterns disappear, while the fabric's pattern contours remain accentuated, as depicted in (a). It is worth nothing that the color of the reflective surface can influence the shape of Turing patterns, whereas the amount of D_Δ does not affect the shape of Turing patterns. In Figure (b), the weakening of Turing patterns on the upper background of the fabric under the Original condition is observed when applying Condition I. This suggests that the amount of D_Δ may potentially control the behavior of Turing patterns. Figure (c) shows that the system remains invariant to D_Δ. Concerning the variable K, even if the color of the surface changes, Turing patterns are consistently generated. However, the color and bleeding of $\mathbf{P}(x,y)$ undergo significant changes. Therefore, we expect the differences in K will emphasize Turing patterns emergence. Finally, in Figure (d), variations in K lead to changes in the color of some contours, yet consistent generation of Turing patterns is observed in all cases. Thus, in this pattern generation process, the reaction and diffusion terms attributed to $\mathbf{R}(x,y)$ are significant, resulting in Turing patterns that are unaffected by the diffusive components or coloration of the reflective surface.

8. Conclusion

This paper successfully demonstrated that Pixel Feedback Animation (PFA) can be effectively modeled as a reaction-diffusion system with three variables, utilizing RGB channels through a comprehensive analysis of the projector-camera system. The investigation further revealed that the reaction and diffusion terms in this model encompass components from direct reflection on the reflective surface, subsurface scattering, and those related to target image generation in the Bubble effect.

Through the utilization of our implemented simulator, we have showcased the potential of image processing techniques and parameters in manipulating the emergence of Turing patterns, particularly leveraging subsurface scattering and the reflectance of the surface. While the presented image processing and parameters serve as examples, it is important to acknowledge the possibility of other techniques and parameters dramatically altering Turing pattern expression based on reflective properties. Nevertheless, the study underscores the intricate balance of factors from target image generation and reflective properties in PFA's reaction and diffusion terms, influencing the manifestation of Turing patterns. In light of this complexity, the challenge arises in attempting to employ identical image processing and parameters for manipulating Turing patterns in objects with varying reflective properties.

Future research directions suggest exploring processing techniques such as normalization of captured images to address diverse reflective properties and investigating generic methods for reliably manipulating the emergence of Turing patterns across a range of scenarios.

References

[AK10a] AMANO T., KATO H.: Appearance control by projector camera feedback for visually impaired. *IEEE Computer Society Conference on Computer Vision and Pattern Recognition - Workshops, CVPRW 2010* (jun 2010), 57–63. doi:10.1109/CVPRW.2010.5543478. 1

[AK10b] AMANO T., KATO H.: Appearance control using projection with model predictive control. 2832–2835. doi:10.1109/ICPR.2010.694. 1

[ALY08] ALIAGA D. G., LAW A. J., YEUNG Y. H.: A virtual restoration stage for real-world objects. *ACM Trans. Graph. 27*, 5 (dec 2008). doi:10.1145/1409060.1409102. 1

[Ama12] AMANO T.: Shading illusion: A novel way for 3-d representation on paper media. pp. 1–6. doi:10.1109/CVPRW.2012.6239192. 1

[Ama13] AMANO T.: Projection based real-time material appearance manipulation. *IEEE Computer Society Conference on Computer Vision and Pattern Recognition Workshops* (06 2013), 918–923. doi:10.1109/CVPRW.2013.135. 1

[Ama16] AMANO T.: Coded facial expression. doi:10.1145/2988240.2988243. 1

[Ama19] AMANO T.: Manipulation of material perception with light-field projection. vol. 10997, International Society for Optics and Photonics, SPIE, p. 1099706. doi:10.1117/12.2522214. 1

[AOSS06] ASHDOWN M., OKABE T., SATO I., SATO Y.: Robust content-dependent photometric projector compensation. In *Conference on Computer Vision and Pattern Recognition Workshop* (USA, 2006), CVPRW '06, IEEE Computer Society, p. 6. doi:10.1109/CVPRW.2006.172. 1

[ASH18] AMANO T., SATO I., HIROTO N.: Japanese patent jp,2018-022287,a, 2 2018. 1

[BBG*13] BERMANO A., BRÜSCHWEILER P., GRUNDHÖFER A., IWAI D., BICKEL B., GROSS M.: Augmenting physical avatars using projector-based illumination. *ACM Trans. Graph. 32*, 6 (Nov. 2013), 189:1–189:10. doi:10.1145/2508363.2508416. 1

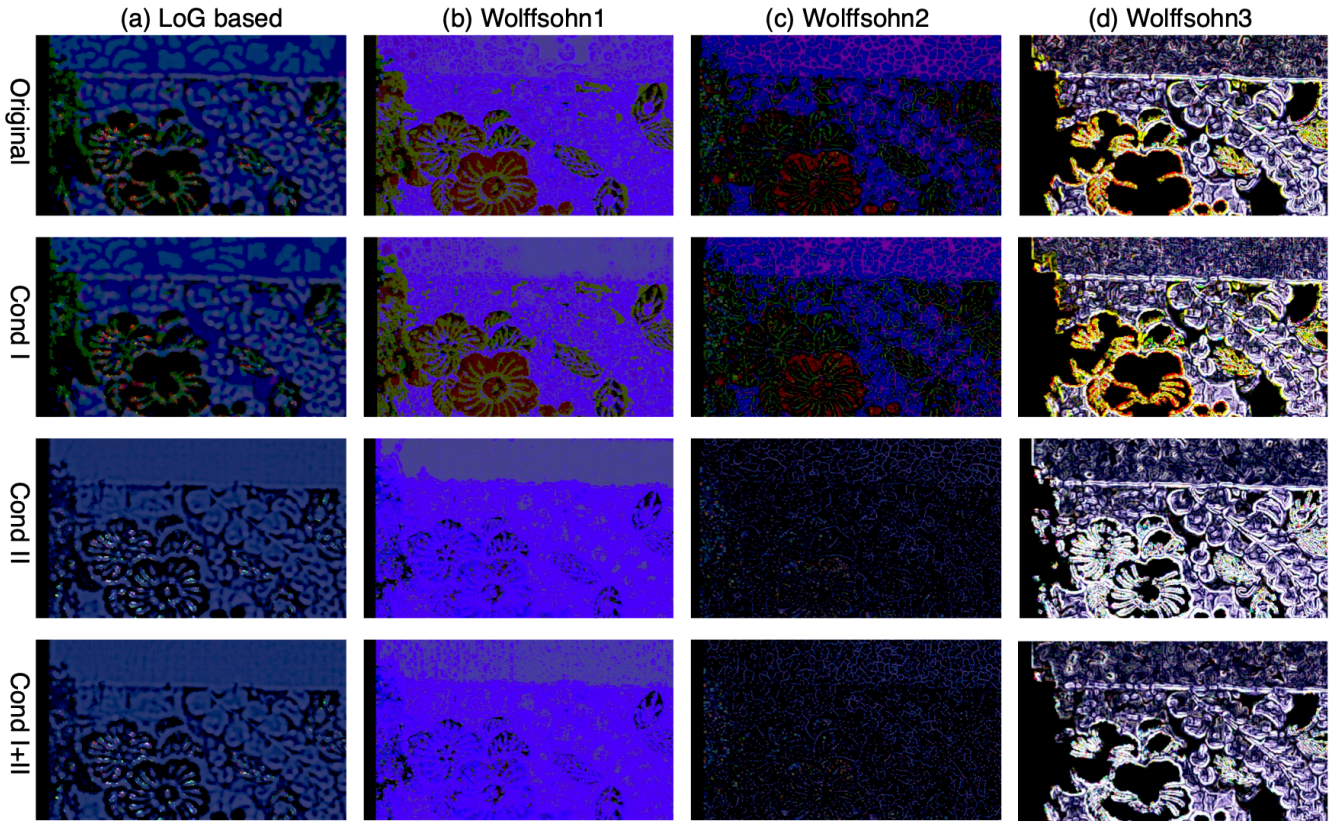

Figure 7: *Turing Pattern Control. This figure illustrates the manipulation of Turing pattern expression under various conditions. In (a), the coloration of the reflective surface influences pattern expression, while* D_Δ *presence does not. In (b),* D_Δ *potentially controls pattern expression. In (c),* D_Δ *remains invariant. For* K*, changes in the reflective surface's color highlight differences in* K*, but Turing patterns persist. In (d), Turing patterns are consistently generated, unaffected by surface color or diffusive components in this pattern generation.*

[GI18] GRUNDHÖFER A., IWAI D.: Recent Advances in projection mapping algorithms, hardware and applications. *Computer Graphics Forum 37*, 2 (2018), 654–675. doi:10.1111/cgf.13387. 1

[GPM89] GARCIA C. E., PRETT D. M., MORARI M.: Model predictive control: Theory and practice - a survey. *Autom. 25*, 3 (1989), 335–348. 4

[GPNB04] GROSSBERG M., PERI H., NAYAR S., BELHUMEUR P.: Making one object look like another: controlling appearance using a projector-camera system. *IEEE Computer Society Conference on Computer Vision and Pattern Recognition, 2004. CVPR 2004. 1* (2004), 452–459. doi:10.1109/CVPR.2004.1315067. 1

[HSW85] HAUSLER G., SECKMEYER G., WEISS T.: Chaos and cooperation in nonlinear pictorial feedback. In *Annual Meeting Optical Society of America* (1985), Optica Publishing Group, p. WT9. doi:10.1364/OAM.1985.WT9. 2

[KFSN16] KAWABE T., FUKIAGE T., SAWAYAMA M., NISHIDA S.: Deformation Lamps. *ACM Transactions on Applied Perception 13*, 2 (2016), 1–17. arXiv:1509.08037, doi:10.1145/2874358. 1

[MTK16] MIYAGAWA I., TANIGUCHI Y., KINEBUCHI T.: [paper] radiometric compensation using color-mixing matrix reformed from light transport matrix. *ITE Transactions on Media Technology and Applications 4*, 2 (2016), 155–168. doi:10.3169/mta.4.155. 5

[PBG*05] PRADEEP S., BILLY C., GAURAV G., MARSCHNER S. R., MARK H., MARC L., LENSCH H. P. A.: Dual photography. *ACM Transactions on Graphics 24*, 3 (07 2005), 745–755. doi:10.1145/1073204.1073257. 4

[RWLB01] RASKAR R., WELCH G., LOW K.-L., BANDYOPADHYAY D.: Shader lamps: Animating real objects with image-based illumination. *Proceedings of the 12th Eurographics Workshop on Rendering Techniques* (2001), 89–102. 1

[SIS11] SHIMAZU S., IWAI D., SATO K.: 3D high dynamic range display system. *2011 10th IEEE International Symposium on Mixed and Augmented Realityrnational Symposium on Mixed and Augmented Reality* (oct 2011), 235–236. doi:10.1109/ISMAR.2011.6092393. 1

[SM92] SCHEPERS H., MARKUS M.: Two types of performance of an isotropic cellular automaton: stationary (turing) patterns and spiral waves. *Physica A: Statistical Mechanics and its Applications 188*, 1 (1992), 337–343. doi:10.1016/0378-4371(92)90277-W. 3

[Tur52] TURING A. M.: The chemical basis of morphogenesis. *Philosophical Transactions of the Royal Society B237* (1952), 37–72. 3

[WMR07] WOLFFSOHN J. S., MUKHOPADHYAY D., RUBINSTEIN M.: Image enhancement of real-time television to benefit the visually impaired. *American Journal of Ophthalmology 144*, 3 (2007), 436 – 440.e1. doi:10.1016/j.ajo.2007.05.031. 5